ChemPubSoc Europe

DOI: 10.1002/chem.201903744

CHEMISTRY A European Journal Full Paper

Nanoparticles

Reactivity of ZrO(MFP) and ZrO(RP) Nanoparticles with $LnCl_3$ for Solvatochromic Luminescence Modification and pH-Dependent Optical Sensing**

Tobias Wehner,[b] Joachim Heck,[c] Claus Feldmann,[c] and Klaus Müller-Buschbaum*[a, b]

Abstract: The luminescence of the inorganic–organic hybrid nanoparticles ZrO(MFP) (MFP = methylfluorescein phosphate) and ZrO(RP) (RP = resorufin phosphate) was modified by addition of different rare earth halides $LnCl_3$. The resulting composite materials form dispersible nanoparticles that exhibit modified nanoparticle fluorescence depending on the rare earth ion. The resulting chromaticity of the luminescence is further variable by the employment of different solvents for ZrO(MFP)-based composite systems. The strong solvatochromic effect of the MFP chromophore leads to different luminescence chromaticities of the composite materials between green, yellow, and blue in THF, toluene, and dichloromethane, respectively. The luminescence of ZrO(RP)-based composite particles can be modified between the red and blue spectral regions in dependence on the applied reaction temperature. Beside a luminescence shift that is derived from nanoparticle modification by $LnCl_3$, a strong turn-on effect of ZrO(RP) particles results after contact with different Brønsted acids and bases in combination with a respective chromaticity shift. Both effects enable the potential employment of such particles as highly sensitive optical pH sensors.

Introduction

Luminescent sensors have attracted tremendous attention in recent years, since photoluminescence processes result in an analytical signal with high sensitivity and easy accessibility.[1] For this purpose, different sensing modes such as the luminescence intensity or lifetime can be exploited. Especially sensors based on fluorescent dyes have been used for a wide range of applications in chemical analysis, biological research, and clinical diagnostics.[2] The development of composite nanoparticles based on fluorescent luminophores allows one to add further advantageous characteristics to the luminescence properties of the dye.[3] For instance, nanoparticulate sensors can be modified with a biocompatible matrix that enables the nanoparticles to be used in living cells and can prevent potential interference of the dye with the cellular environment.[4] Such systems are widely used as agents for optical imaging techniques such as different tomographic methods[5] and luminescence imaging[6] with applications reaching from noninvasive diagnosis to in vivo observations of vital functions.[7] Furthermore, several luminophores can be included in a one-particle system, which suggests applying these systems as ratiometric sensors.[4c–e]

Luminescent nanosensors can be used for the detection of a variety of different targets, which include metal cations,[8] solvents,[9] gases,[10] and physical parameters such as temperature[1a,11] and pH value.[12] Sensors for metal cations include, among others, silole nanoparticles for the determination of Cr^{VI}[13] and NaYF:Yb^{3+}/Er^{3+} upconverting nanoparticles for the detection of Hg^{II}.[14] A large number of biocompatible sensors based on organic dyes can be used to detect metal cations that play an important role in metabolic processes (e.g., Zn^{2+}, Fe^{2+}, Fe^{3+}, Mn^{2+}) in living cells.[15] Temperature-dependent nanoparticle-based sensors include quantum dots,[16] upconverting nanoparticles that are codoped with lanthanide ions,[17] and nanoparticles based on fluorescent dyes.[18] ZrO(FMN) (FMN = flavin mononucleotide) nanoparticles represent the latter category and show distinct luminescence changes for different reaction temperatures.[19] Nanoparticles based on dyes are typically synthesized by coprecipitation of the luminophore and a host matrix material.[20] The combination of suitable starting components allows, for instance, the design of fluorescent nanothermometers that are able to determine the temperature of a single living cell.[11b] Nanoparticle composites

[a] Prof. Dr. K. Müller-Buschbaum
Institute of Inorganic and Analytical Chemistry
Justus-Liebig University Giessen
Heinrich-Buff-Ring 17, 35390 Giessen (Germany)
E-mail: kmbac@uni-giessen.de

[b] Dr. T. Wehner, Prof. Dr. K. Müller-Buschbaum
Institute of Inorganic Chemistry, Julius-Maximilians University Würzburg
Am Hubland, 97074 Würzburg (Germany)

[c] Dr. J. Heck, Prof. Dr. C. Feldmann
Institute of Inorganic Chemistry, Karlsruhe Institute of Technologie (KIT)
Engesserstrasse 15, 76131 Karlsruhe (Germany)

[**] MFP = methylfluorescein phosphate, RP = resorufin phosphate.

Supporting information and the ORCID identification number(s) for the author(s) of this article can be found under: https://doi.org/10.1002/chem.201903744.

for pH sensing can, for instance, be based on CdTe nanocrystals,[21] modified carbon nanodots,[22] or functionalized acrylamide monomers.[23] Depending on their composition, these compounds can be applied for pH detection in solvents and in living cells. Beside nanoparticle-based sensors, different lanthanide-based compounds, such as metal–organic frameworks (MOFs), can also be applied for the detection of targets such as distinct metal ions[24] and molecules[25] as well as environmental conditions such as pH[26] value and temperature.[27] The sensing effect is caused by interaction of the framework with the analyte, leading to changes in the luminescence properties of the MOF.[28]

The interaction of a target molecule with a luminescent sensor can have different effects on the luminescence properties of the sensor. Numerous sensors are based on a change in luminescence intensity after contact with an analyte.[1c,29] Some detectors show an increase in their luminescence intensity after interaction with a target (turn-on sensors).[30] In contrast, the binding between sensor and target molecule can result in a significant decrease of the luminescence intensity or in complete quenching (turn-off sensors).[31] Multiple turn-on/turn-off systems that contain fluorescent dyes are based on a photoinduced electron transfer mechanism.[1c,32] Besides intensity-based sensors, the interaction of a target with a luminescent detector system can result in a chromaticity shift of the resulting luminescence through internal charge-transfer processes.[1c,29,33]

Herein, we present the synthesis and properties of composite materials based on ZrO(MFP) (MFP = methylfluorescein phosphate) and ZrO(RP) (RP = resorufin phosphate) nanoparticles and rare earth halides. The resulting nanocomposites exhibit various luminescence properties dependent on the particular fluorophore and the rare earth ion. On the basis of the respective dye, these properties can be influenced with respect to the luminescence chromaticity by variation of the dispersion medium or the reaction temperature. Furthermore, interaction of ZrO(RP) nanoparticles with Brønsted acids or bases leads to an intensive turn-on effect of the luminescence intensity. Therefore, ZrO(RP) shows high potential for applications as a pH detector.

Results and Discussion

General considerations

We selected the luminescent inorganic–organic hybrid nanomaterials ZrO(MFP) and ZrO(RP) as starting components for $LnCl_3$-functionalized composite materials. Nanoparticles of general composition $[ZrO]^{2+}[R_{dye}OPO_3]^{2-}$ are versatile luminescent materials that can be synthesized by a simple one-pot reaction of $ZrOCl_2$ with the sodium salt or acid of the corresponding dye. The synthesis yields nanoparticles with 30–40 nm diameter in a stable colloidal suspension (Supporting Information: Table S1, Figures S1–S4).[3,4b] In contrast to other nanoparticulate luminescent materials such as quantum dots, these compounds show high biocompatibility and are therefore suited as biomarkers for in vivo and in vitro applications.[4b] Whereas the functional organic anion $[R_{dye}OPO_3]^{2-}$ determines the luminescence properties of the composite material, the $[ZrO]^{2+}$ cation enables the preparation of insoluble nanoparticles (Supporting Information: Table S2). To synthesize inorganic–organic hybrid nanoparticles, various dyes such as phenylumbelliferon phosphate (PUP), flavin mononucleotide (FMN), methyl fluorescein phosphate (MFP), resorufin phosphate (RP), and Dyomics-647 uridine triphosphate (DUT) could be applied to achieve different luminescence colors that cover the whole visible spectral region (PUP: blue; FMN, MFP: green; RP: red; DUT: infrared).[34] The ZrO(MFP) and ZrO(RP) nanoparticles that were used as starting components for the composite materials in this work and their respective luminescence properties are depicted in Figure 1 (see also Supporting Information: Figure S5).

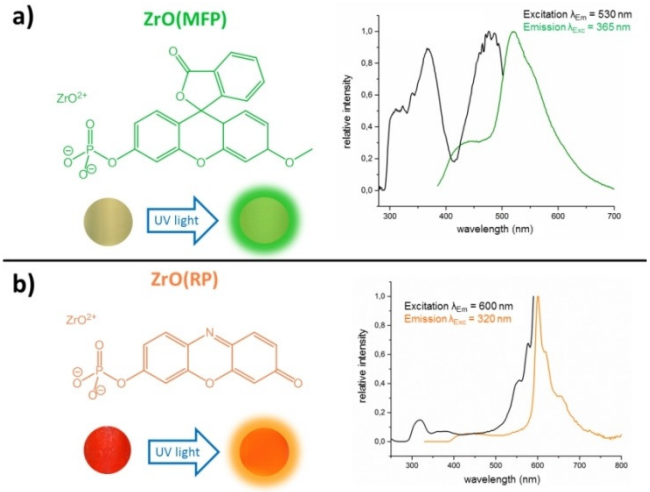

Figure 1. Composition and constituents (left) as well as excitation and emission spectra (right) of ZrO(MFP) (a) and ZrO(RP) (b) nanoparticles.

We have previously described the functionalization of green-emitting ZrO(FMN) nanoparticles with rare earth chlorides.[19] The resulting composite materials show luminescence properties that differ from the fluorescence of the original nanoparticles in dependence on the applied rare earth ion and the reaction temperature. Suitable reaction conditions lead to the preparation of white-light-emitting materials with a high color rendering index (CRI). Herein, we selected ZrO(MFP) and ZrO(RP) as starting components for $LnCl_3$-modified composite materials in order to widen the range of available functionalities in the chromophore in addition to different photoluminescence chromaticity.

While MFP exhibits a green chromaticity comparable to that of FMN, it additionally shows a strong solvatochromic effect.[35] Thus, the luminescence of the resulting composite materials $LnCl_3$@ZrO(MFP) [Ln = La (**1**), Eu (**2**), Ho (**3**)] can be varied in dependence on the particular dispersion medium.

RP shows intense orange luminescence and therefore enables the establishment of another luminescence chromaticity in the resulting composite materials compared to the FMN- and MFP-containing composites. Similar to ZrO(FMN)-based composite particles, the YCl_3-modified composite YCl_3@ZrO(RP)

(**4**) can exhibit a luminescence chromaticity between the red and blue spectral regions in dependence on the applied modification temperature.

Nanocomposites with solvatochromic luminescence properties based on ZrO(MFP)

For preparation of solvatochromic, luminescent composite particles $LnCl_3$@ZrO(MFP) [Ln = La (**1**), Eu (**2**), Ho (**3**)], dispersions of ZrO(MFP) nanoparticles in different solvents were treated with equimolar amounts of anhydrous $LnCl_3$. To examine the solvatochromic effect of the resulting materials, we utilized THF, toluene, and dichloromethane, which show distinct differences in polarity, as dispersion media. The reaction of the starting components took place at room temperature and yielded composite materials **1**–**3** as orange dispersions. These materials exhibit luminescence properties that are visible on excitation with UV light and significantly differ from the fluorescence of the original MFP. Since the structurally similar ZrO(FMN) particles show a distinct dependence of their luminescence properties on the reaction temperature,[19] the synthesis of ZrO(MFP)-based composite materials was conducted at higher temperatures (85 °C in THF, 130 °C in toluene, 80 °C in dichloromethane). However, a higher reaction temperature did not result in a change of the luminescence properties in THF and dichloromethane. In toluene, decreased luminescence intensity was observed, which could be assigned to degradation of the ZrO(MFP) particles at higher temperatures.

The modification of ZrO(MFP) with $LnCl_3$ leads to a distinct shift of the green luminescence of the resulting composites **1**–**3** to white, as well as to the blue or yellow region of the visible spectrum. The resulting luminescence chromaticity depends on the solvent and the lanthanide ion. For instance, La^{3+}-containing composite **1** exhibits light blue luminescence in THF, light green luminescence in toluene, and turquoise-green luminescence in dichloromethane. $EuCl_3$@ZrO(MFP) (**2**) can exhibit a white-yellow (THF), green-yellow (toluene), or turquoise-green (dichloromethane) luminescence color, whereas $HoCl_3$-modified material **3** shows varying luminescence chromaticity only in the green spectral region in different solvents. Figure 2 shows photographs depicting the different luminescence properties of the ZrO(MFP)-based composite materials.

The observed shift of the chromaticity can be assigned to different changes in the photoluminescence spectra of composite materials **1**–**3**, which are shown in Figure 3 together with excerpts of the CIE diagram, indicating the resulting luminescence chromaticity. The emission properties of the resulting luminescence are based on the MFP fluorescence band (λ_{max} = 518 nm), which is modified by different processes after contact with $LnCl_3$.

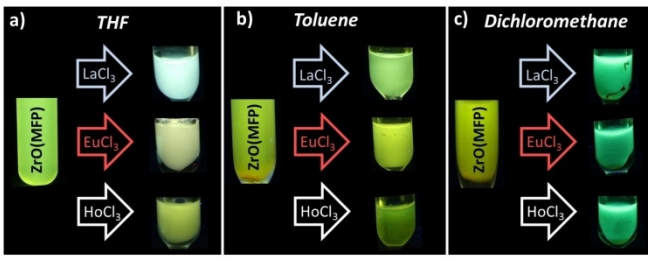

Figure 2. Fluorescence of ZrO(MFP) and of $LnCl_3$@ZrO(MFP) composite particles [Ln = La (**1**), Eu (**2**), Ho (**3**)] as dispersions in THF (a), toluene (b), and dichloromethane (c) on excitation by UV light (λ_{Exc} = 365 nm).

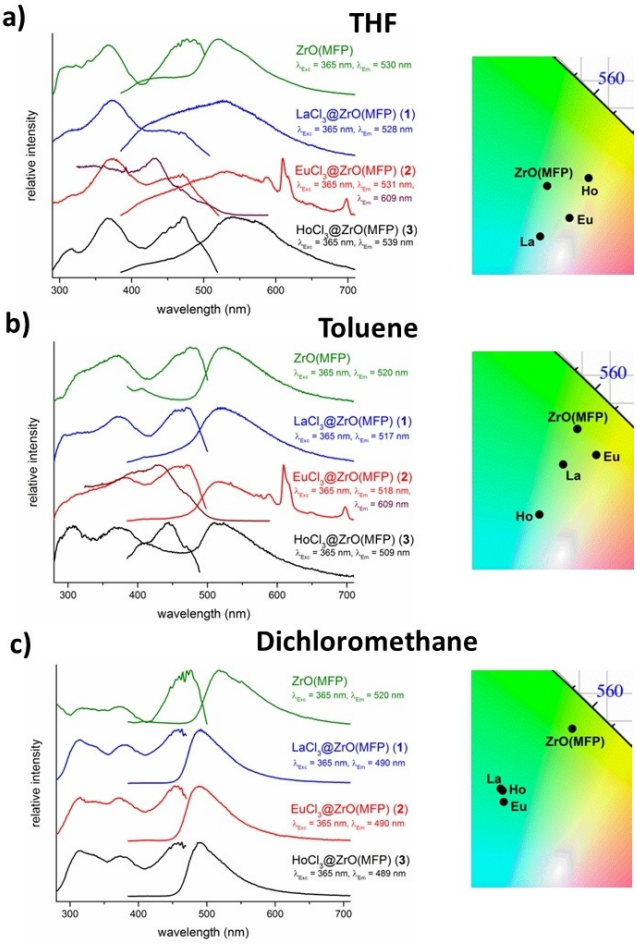

Figure 3. Excitation and emission spectra of ZrO(MFP) and of $LnCl_3$@ZrO(MFP) composite particles [Ln = La (**1**), Eu (**2**), Ho (**3**)] as dispersions in THF (a), toluene (b), and dichloromethane (c) as well as excerpts of the CIE diagram with resulting chromaticity [λ_{Exc} = 365 nm, λ_{Em} = 530 nm (ZrO(MFP), a), 520 nm (ZrO(MFP), b,c), 528 nm (**1**, a), 517 nm (**1**, b), 490 nm (**1**, c), 531, 609 nm (**2**, a), 518, 609 nm (**2**, b), 490 nm (**2**, c), 539 nm (**3**, a) 509 nm (**3**, b), 489 nm (**3**, c)].

Modification of ZrO(MFP) with $LnCl_3$ in THF leads to band broadening of the chromophore's fluorescence at higher and lower energies. Depending on the lanthanide ion, one of the two processes is dominant, leading to a blue- or redshift, respectively. For La^{3+}-based composite **1**, a bathochromic shift of the MFP fluorescence to λ_{max} = 526 nm can be observed. Furthermore, the luminescence band is significantly broadened in the blue spectral region, and this leads to a similar luminescence intensity of the MFP band and the band at higher energy. This results in a chromaticity of composite **1** in THF close to the ideal white point with a calculated CRI of 69.

In contrast, $HoCl_3$-containing composite material **3** shows band broadening in the red spectral region, whereas the

shoulder in the blue region remains nearly unaltered. This leads to a bathochromic shift of the MFP fluorescence and to chromaticity in the yellow spectral region.

For $EuCl_3$@ZrO(MFP) (**2**), the band broadening takes place in the red and blue spectral regions to similar extents. However, in addition to the broad MFP fluorescence, significant 4f–4f emission bands of Eu^{3+} can be detected. The transition $^5D_0 \rightarrow {}^7F_2$ ($\lambda = 610$ nm) has the highest intensity, which increases the luminescence intensity in the red spectral region and leads to a chromaticity near the white point with a high CRI of 78. The presence of the Eu^{3+} emission can be explained by binding of the fluorophore or the solvent THF to the lanthanide ion. The excitation exhibits a broad band at $\lambda_{max} = 432$ nm, indicating energy transfer to the Eu^{3+} ion through an antenna effect. The energy transfer can be caused by MFP as sensitizer, as THF does not exhibit transitions in the respective energy region. However, the maximum in excitation for the Eu^{3+} emission at 609 nm does not simply match with the maximum of the free fluorophore, and this may also indicate a more complex process. Additionally, a direct 4f–4f excitation of Eu^{3+} can be detected with low intensity ($\lambda_{max} = 392$ nm).

Thus, the modification of ZrO(MFP) in THF results in different luminescence chromaticity depending on the rare earth ion in the composite. The luminescence band in the blue wavelength region, which can be assigned to an internal charge-transfer process between the chromophore and the Lewis acid $LnCl_3$, indicates binding between the two components through the donor function of the organic anion. The interaction of MFP with a lanthanide ion results in lower electron density of the fluorophore and thus in energetic destabilization of the LUMO of MFP, which causes a blueshift.[1b,c,36] The magnitude of the blueshift is dependent on the electronegativity, Lewis acidity, and the size of the metal ion. The three selected lanthanides have different ionic diameters (La^{3+}: 106 pm, Eu^{3+}: 95.0 pm, Ho^{3+}: 89.4 pm), which decrease with increasing atomic number due to the lanthanide contraction.[37] Therefore, composites **1**–**3** show distinct variations in the intensity of the chromophore band. The broad band spanning to the red spectral region can be assigned to the MFP fluorescence and shows differences in intensity according to the lanthanide ion.[38] The intensity of both intramolecular charge transfer and fluorescence of fluorescein-based dyes can also be influenced by the polarity of the solvent [ε(298 K) = 7.58 (THF), 2.38 (toluene), 8.93 (dichloromethane)].[39] Consequently, not only the lanthanide ion but also THF as solvent have distinct influences on the intensity of all participating luminescence processes.

The modification of ZrO(MFP) in toluene leads to a luminescence modification that varies from the luminescence of the composite materials in THF. All composite materials **1**–**3** show only band broadening of the MFP fluorescence at higher energies, whereas the emission band shows no significant changes in the red spectral region. The dipole moment in the excited state of fluorescein is larger than that in its ground state. Therefore, a polar solvent like THF leads to stabilization of the higher polarity of the excited state that results in a smaller energy gap between HOMO and LUMO, causing a redshift of the emission.[39a,c] Thus, the band broadening at lower energies cannot be observed for toluene and dichloromethane. The emission band in the blue spectral region is most intense for Ho^{3+}-containing composite **3** and thus leads to a stronger blueshift compared with composites **1** and **2**. In accordance with the observation for the $EuCl_3$-modified particles in THF, composite **2** exhibits significant Eu^{3+} emission bands. Toluene as a noncoordinating solvent cannot establish considerable binding, and thus coordination to the Lewis acidic Ln^{3+} ions. Therefore, energy transfer to Eu^{3+} occurs via the MFP fluorophore, which acts as sensitizer. The additional red Eu^{3+} emission in the two-chromophore system **2** leads to a bathochromic shift of the emission to the yellow spectral region.

In contrast to the composite materials in THF and toluene, dispersions of $LnCl_3$@ZrO(MFP) [Ln = La (**1**), Eu (**2**), Ho (**3**)] in dichloromethane cannot be optically distinguished by their chromaticity. The chromaticity of the MFP dye is shifted from green to turquoise for all three lanthanide ions. Unlike the behavior in THF and toluene, the hypsochromic shift is not caused by band broadening, but by a shift of the complete emission band from $\lambda_{max} = 518$ nm to $\lambda_{max} = 490$ nm, whereas the band width is slightly reduced. Additionally, no 4f–4f transitions of Eu^{3+} can be detected in Eu^{3+}-containing composite **2**, and this indicates the absence of an antenna effect. We assign this to a reduction of the energy of the fluorophore excited states to a point below the Eu acceptor level, which thus precludes energy transfer to Eu.

Fluorescein-based chromophores show a strong solvatochromic effect that to some extent depends on the polarity of the solvent. The fluorophore can exist in cationic, monoanionic, or dianionic form,[35,40] which show differences in their luminescence properties concerning the emission maxima and the bandwidth. Whereas fluorescein exists in a protonated form in toluene, it exhibits anionic character in the polar solvents dichloromethane and THF. In general, deprotonation of the fluorophore leads to a redshift of the luminescence band. Therefore, the polarity and acidity of the solvent determine the luminescence properties of the composite materials.

For additional analysis of the composite systems, material **1** was analyzed by IR spectroscopy. IR spectroscopic analysis of composite material **1** dried from a dispersion in THF confirmed the presence of the nanoparticles in the resulting composite. The MFP component of the microparticle can be identified by the P–O valence vibration at 1011 cm^{-1} and the C=C deformation vibrations (1259 cm^{-1}, 790 cm^{-1}). Additionally, the C–H valence vibration of the solvent THF, which could be detected at 2963 cm^{-1}, indicated remnants of THF in the composite materials that could not be removed under vacuum.

Nanocomposites with temperature-dependent luminescence properties based on ZrO(RP)

For the synthesis of a composite material with chromaticity in the red wavelength region, water-free YCl_3 was added to a dispersion of ZrO(RP) in pyridine under inert-gas conditions. The composite material YCl_3@ZrO(RP) (**4**) showed only a small change of the luminescence properties after reaction at room temperature. Therefore, the reaction mixture was heated to

100 °C. Increasing the reaction temperature leads to a strong hypsochromic shift of the RP emission from red via magenta to blue. Thus, system **4** shows a similar behavior to $LnCl_3$@ZrO(FMN) composite materials, which also exhibit a temperature-dependent blueshift of the chromaticity.[19] Similar to the luminescence behavior of the modified ZrO(MFP) particles, the emission band of RP in the orange spectral region constitutes the basis of the emission properties of the composite material. Binding of Y^{3+} to the dye-containing nanoparticle results in modification of the emission band, which can result in a shift of the emission maximum or in band broadening. The fluorescence of the dye and that of the composite material can be excited in the UV and in the visible spectral region and thus is observable in daylight (see Figure 4). In addition to this temperature-dependent blueshift, a hypsochromic shift of the chromaticity could also be observed after storage of the composite materials in evacuated ampoules. Thus, the ZrO(RP)-based particles exhibit high sensitivity to exterior parameters such as pressure and temperature, and at 77 K (liquid nitrogen) the particle dispersions lose their luminescence over several days due to slow degradation, whereas ZrO(MFP)- and ZrO(FMN)-based composites did not show a comparable effect. Altogether, ZrO(RP)-based particles show significant luminescence modification of the composite materials for different stimuli.

Reaction of ZrO(RP) with YCl_3 at room temperature led to band broadening of the RP emission in the red wavelength region (600–680 nm) with a broad banded shoulder at λ_{max} = 635 nm, whereas the absolute emission maximum of the fluorescence is detected at λ_{max} = 605 nm. The band broadening correlates with an increasing intensity of the excitation band at lower energy and results in a bathochromic shift of the luminescence to the red spectral region. Heating of the dispersion of composite particles to 100 °C results in further modification

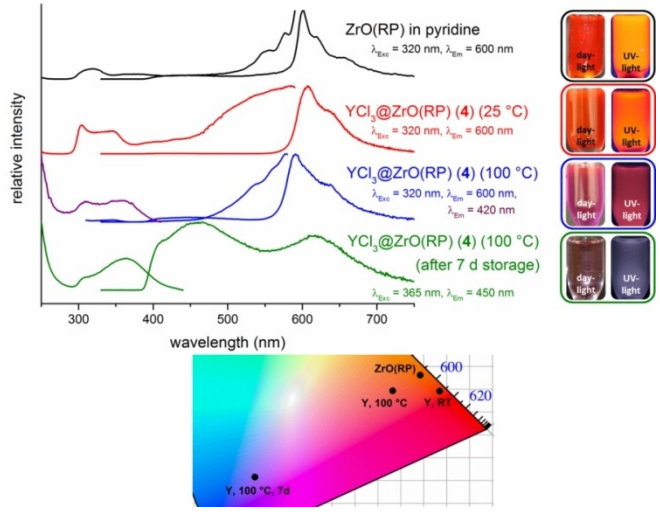

Figure 4. Excitation and emission spectra of ZrO(RP) and YCl_3@ZrO(MFP) composite particles (**4**) as dispersions in pyridine for different reaction temperatures and storage conditions (left, λ_{Exc} = 320 and 365 nm, λ_{Em} = 600 nm (ZrO(RP) in py) and 420 and 450 nm for **4**), corresponding photographs in daylight and on excitation by UV light (λ_{Exc} = 365 nm, right), and excerpts of the CIE diagram with resulting chromaticities (bottom).

of the luminescence properties. Two processes that lead to a hypsochromic chromaticity shift are detectable: first, the fluorescence band is hypsochromically shifted from λ_{max} = 605 nm to λ_{max} = 590 nm without changing its bandwidth. Second, an additional emission band in the blue spectral region with λ_{max} = 375 nm occurs. Combination of both processes leads to a chromaticity shift resulting in a magenta luminescence color. Storage of the composite particles in evacuated reaction vessels for 7 d also leads to a significant increase of the emission band in the blue spectral region. Additionally, a band at lower energy with λ_{max} = 615 nm and a broader band width than the original RP fluorescence can be observed. The luminescence shows a significantly smaller amount of the red fluorescence band and thus indicates degradation of the particles.

To investigate the composite character of **4**, the dispersion (reaction temperature 100 °C) was analyzed by SEM, energy-dispersive X-ray spectroscopy (EDX), dynamic light scattering (DLS), and IR spectroscopy. The particle size and size distribution were determined by DLS. The composite-particle size is distributed between 800 and 1100 nm (85% between 1000 and 1100 nm, see Supporting Information: Figure S6). In contrast, the size of the pure ZrO(RP) nanoparticles is between 20 and 40 nm.[34] Thus, modification with $LnCl_3$ leads to a significant increase of size and aggregation of the particles. SEM images show particles with diameters of about 1 μm, which aggregate to particles of several micrometers in length after drying the dispersions, in confirmation of the DLS results. Thus, the ZrO(RP)-based composite materials form large but floatable nanoparticulate aggregates, that retain their luminescence properties in dispersion.

EDX analysis of the dispersions show a Y amount of 3.9% and a Cl amount of 6.3%, confirming the presence of both yttrium and chlorine from YCl_3 in the formed composite material (see Supporting Information: Table S3). P and Zr, the elements representative for the ZrO(RP) nanoparticles, could not be detected. This indicates a presumable core–shell character of the formed composite materials. Due to its low penetration depth, the electron beam can only interact with the outer lanthanide-containing shell. Since Zr and P could not be detected, it can be concluded that core–shell systems with a ZrO(RP) core and a shell constituted by Y^{3+} and Cl^- are formed. This conclusion coincides with the analysis of the similar particle system $LnCl_3$@ZrO(FMN), for which an analogous core–shell structure could be confirmed by comparison of EDX and X-ray fluorescence data.[19]

IR spectroscopic analysis of dried dispersions of YCl_3@ZrO(RP) (**4**) showed the presence of all vibration bands characteristic of the organic RP unit. For instance, the C=C deformation vibration of the aromatic system (1260, 800 cm^{-1}) and the P–O valence vibration of the phosphate group (1050 cm^{-1}) are detectable and thus confirm the presence of RP in the composite material (see Supporting Information: Figure S1).

Summing up, the ZrO(RP)-based composite **4** shows similarities in its composition and luminescence behavior to the previously described particle system ZrO(FMN)@$LnCl_3$.[19] Both composites form core–shell systems with a nanoparticle core and a

lanthanide-containing shell. The luminescence properties of these systems can be modified in dependence on the reaction temperature, whereby higher temperature leads to a hypsochromic chromaticity shift and instability of the particles if heated too far. The chromaticity shift enables the generation of luminescence colors in a broad range between the red and blue spectral regions for RP-containing particles. In comparison with the MFP-based materials **1**–**3**, this exchange of the nanoparticle component enables different luminescence properties and a different temperature- and solvent-dependent behavior of the resulting composite materials.

Application of ZrO(RP) nanoparticles as pH detector

Besides the change in luminescence properties after interaction with Lewis acids such as $LnCl_3$, ZrO(RP) nanoparticles show an intensive change of their fluorescence after contact with Brønsted acids or bases. Therefore, the particle system shows potential for application as an optical pH detector. To analyze the detection behavior on contact with acids and bases, a dispersion of ZrO(RP) in pyridine was treated with HCl (1.2 m) and NEt_3. This led to a distinct modification of the luminescence emission intensity, chromaticity, and excitation intensity (see Figure 5a). Addition of HCl to the nanoparticle dispersion does not lead to any significant change of the emission band in terms of emission maxima, bandwidth, or band shape, and the orange fluorescence chromaticity of the unmodified ZrO(RP) particles results. However, a significant increase of the emission intensity can be observed, even by the naked eye.

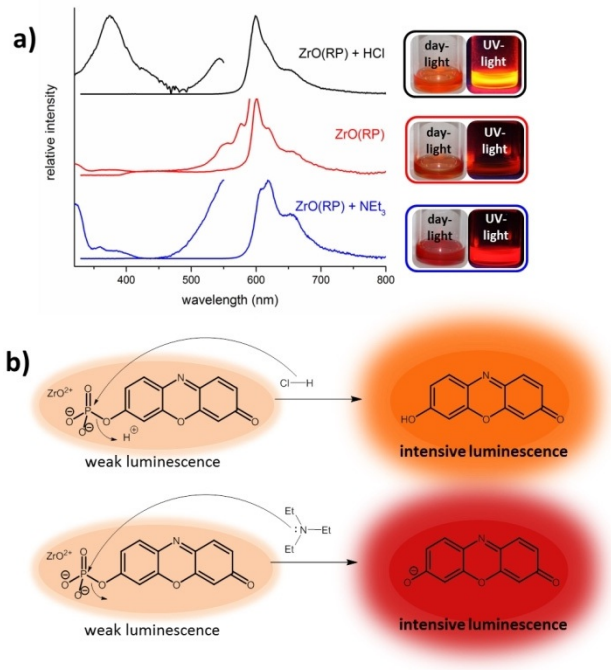

Figure 5. Excitation and emission spectra of ZrO(RP) and of ZrO(RP) after addition of HCl and NEt_3 with corresponding photographs in daylight and on excitation by UV light (λ_{Exc} = 365 nm) (a) and proposed reaction mechanisms for the sensing of HCl and NEt_3 with ZrO(RP) (b).

This intensity increase is accompanied by an additional excitation band at λ_{max} = 375 nm.

Treatment of ZrO(RP) with NEt_3 also results in increased emission intensity. However, this increase in intensity is accompanied by a bathochromic shift of the emission that is caused by band broadening in the red wavelength region with an additional local maximum at λ_{max} = 653 nm and a shift of the absolute emission maximum from 602 to 618 nm. This chromaticity shift is reversible, so that the original chromaticity of ZrO(RP) can be regained by addition of HCl to the nanoparticle dispersion after addition of NEt_3. In contrast, the increase in emission intensity is irreversible.

The strong increase in intensity by more than five orders of magnitude after interaction of ZrO(RP) with HCl or NEt_3 indicates an increase of the electron density of the fluorophore during the sensing procedure. Resorufin-based systems can be employed as turn-on sensors for different target molecules, for example, hydrazine,[41] nitroxyl (HNO),[42] and acetylcholinesterase.[43] Such sensors require functionalization with an electron-withdrawing group that simultaneously acts as receptor for the analyte. The aforementioned sensors are based on the resorufin dye, which is connected to an organic unit by an ester[41,42] or sulfate group,[43] respectively. Functionalization with the electron-withdrawing group generates a strong intensity decrease of the resulting fluorescence of the dye. Reaction with NEt_3 or HCl results in elimination of the electron-withdrawing group and thus in formation of the unmodified fluorophore resorufin. We consider this to be responsible for the significant increase of the luminescence intensity.[41–43] Such an effect was also shown for ZrO(UFP) nanoparticles containing the coumarin derivative umbelliferon phosphate (UFP) as fluorescent dye.[44]

On the basis of this mechanism, a similar sensing mechanism can be suggested for the sensing of Brønsted acids or bases by ZrO(RP). The functionalization of resorufin with a phosphate group that is connected to a zirconyl cation, in principle, results in a luminescence decrease in comparison with the pure resorufin fluorophore that is caused by the electron-withdrawing effect of the zirconyl phosphate group. Reaction with HCl or NEt_3 presumably results in elimination of the phosphate group and formation of the pure resorufin fluorophore (see Figure 5b). This results in a significant intensity increase of the luminescence, since the quenching of the resorufin luminescence by the zirconyl phosphate functionalization is repealed. Thus, the modification of resorufin by zirconyl-phosphate-containing nanoparticles enables the optical detection of nucleophilic molecules by a strong turn-on effect that could not be obtained with the pure fluorophore alone.

The proposed sensing mechanism can explain the intensity increase of the fluorescence after contact with HCl and NEt_3, but does not give any information on why the chromaticity of the fluorophore is only changed after addition of NEt_3 and not after treatment with HCl. It is likely that resorufin is protonated in acidic or neutral environment and is in its anionic form after contact with a Brønsted base. The two species differ in electron density, which could explain the different chromaticity after the sensing procedure of NEt_3.

For the quantitative characterization of pH sensing by ZrO(RP), a dispersion of 3.01 μmol ZrO(RP) in pyridine (0.2 mL) was titrated stepwise with preset amounts and concentrations of base, water, or acid (1 μL each: 7.21 μmol NEt_3, 55.5 μmol H_2O, and 1.21 μmol HCl per step). The absolute emission intensity was detected after each sensing process by integration of the emission spectra under identical instrumental conditions. Figure 6 shows the excitation and emission spectra as well as the integrated emission intensity in dependence on the amount of substance ratio of acid/base and ZrO(RP).

In general, a larger amount of analyte leads to an increase in luminescence intensity, accompanied by a differing increase in dependence on the target molecule. The addition of amounts of 1 μL of analyte to a fixed amount of particles results in different ratios due to the different molar masses of the analytes. For comparison of the results, the intensity increase was described by an exponential fit for all three analytes. Thereby, a calibration for determination of the amount of analyte and the photoluminescence intensity is available.

The addition of 1 μL of NEt_3 to ZrO(RP) results in a sevenfold increase of the absolute emission intensity and can lead to an intensity 16 times higher than the original ZrO(RP) intensity on adding further NEt_3.

Addition of water results in a smaller increase of the emission intensity. Only large amounts of water lead to a significant intensity increase, which we attribute to partial quenching by high vibronic states of water countering the effect of RP release. The intensity increase can be fitted with a biexponential fit for larger amounts of H_2O. In analogy to the titration with NEt_3, a band broadening and, thus, a bathochromic shift of the chromaticity can be obtained. Accordingly, an identical sensing mechanism for both targets can be assumed. Presumably, H_2O acts as a Brønsted base, so that the resorufin fluorophore attains its deprotonated form.

The intensity increase after addition of HCl also proceeds exponentially and leads to an intensity increase up to 13 times the original luminescence intensity. Thus, the intensity increase for titration with HCl is comparable with the increase by NEt_3 addition, however, without a chromaticity change.

Addition of HCl, NEt_3, and H_2O leads to modification of the ZrO(RP) luminescence regarding its absolute emission intensity as well as its chromaticity. Both values can be referenced to the pH value of the system, and this demonstrates potential application of ZrO(RP) as a pH detector.

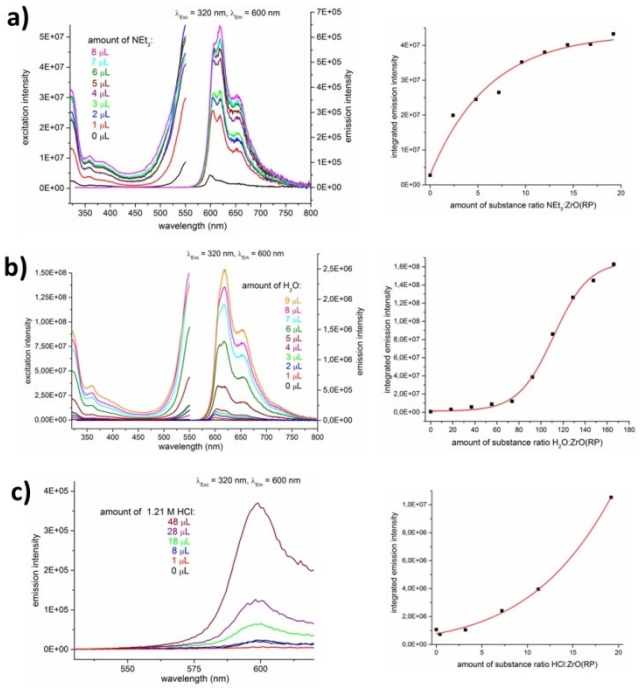

Figure 6. Excitation and emission spectra of ZrO(RP) and ZrO(RP) after addition of different amounts of NEt_3 (a), H_2O (b), and HCl (c) (left; deviation: 0.1 μL) as well as integrated emission intensities of ZrO(RP) in dependence on the amount of substance ratio of NEt_3 (a), H_2O (b), and HCl (c) (right).

Conclusion

Functionalization of the luminescent nanoparticle systems ZrO(MFP) and ZrO(RP) with $LnCl_3$ leads to distinct modification of the nanoparticle fluorescence that is dependent on different chemical and physical conditions. The composite systems $LnCl_3$@ZrO(MFP) [Ln = La (**1**), Eu (**2**), Ho (**3**)] show different luminescence properties dependent on the particular rare earth ion. Due to the strong solvatochromic effect of MFP, these properties are further modifiable by the use of different solvents (THF, toluene, dichloromethane). The resulting composite materials exhibit luminescence properties that are tunable in the visible spectral region between blue, green, yellow, and white-light emission. The core/shell composite system YCl_3@ZrO(RP) can exhibit chromaticity that reaches from the red to the blue spectral region via magenta, in dependence on the applied reaction temperature. Furthermore, unmodified ZrO(RP) nanoparticles are applicable as optical pH sensors for Brønsted acids and bases. The intensive turn-on effect observed can be attributed to the release of RP, which is accompanied by a shift of chromaticity for Brønsted bases by deprotonation. Chromaticity shift and intensity increase are dependent on the applied acid and base and therefore enable an assignment of optical properties to the pH value, for example, for HCl.

Experimental Section

Synthesis and reagents

Reagents: ZrO(MFP) and ZrO(RP) nanoparticles were prepared, as described before, by the reaction of an aqueous solution of $ZrOCl_2 \cdot 8H_2O$ with cyclohexylammonium methylfluorescein phosphate and resorufin phosphorous acid, respectively.[34] La_2O_3 (99.5%, Merck KGaA), Eu_2O_3 (99%, Research Chemicals), Ho_2O_3 (99.9%, Research Chemicals), NH_4Cl (99.5%, Grüssing GmbH), and YCl_3 (99.9%, Strem Chemicals) were used without further purification. Anhydrous lanthanide chlorides were prepared by the ammonium halide route by reaction of Ln_2O_3 (Ln = La, Eu, Ho) with NH_4Cl in concentrated HCl.[45] The reaction was followed by thermal decomposition of the generated salt $[NH_4]_3[LnCl_6]$ and subsequent purification by sublimation.

Synthesis of $LnCl_3$@ZrO(MFP) [Ln = La (1), Eu (2), Ho (3)] composite particles: $LnCl_3$ [3.76 μmol, 922 μg (Ln = La), 972 μg (Ln = Eu), 1.29 μg (Ln = Ho)] was placed in a Duran glass ampoule under argon atmosphere together with 0.5 mL of a dispersion of ZrO(MFP) (1.88 μmol, 1.00 mg) in THF, toluene, or dichloromethane, respectively. The ampoule was repeatedly frozen, evacuated, and thawed to degas the solvent. A reaction that could be detected by visible change of the luminescence properties occurred after 1 h at room temperature. The dispersion and the formed precipitate were separated under inert gas atmosphere and the resulting precipitate was dried under vacuum. IR: $\tilde{\nu}$ = 3460 (w), 2963 (m), 1611 (w), 1456 (w), 1411 (w), 1259 (s), 1082 (s), 1011 (s), 865 (w), 790 cm^{-1} (s).

Synthesis of YCl_3@ZrO(RP) (4) composite particles: YCl_3 (75.3 μmol, 14.7 mg) was placed in a Schlenk flask together with 5.0 mL of a dispersion of ZrO(RP) (75.3 μmol, 30.0 mg) in pyridine under inert gas atmosphere. The reaction mixture was heated under reflux to 100 °C for 24 h. The dispersion was separated from the formed precipitate and the precipitated composite particles were dried under vacuum. elemental analysis (%) calcd for $YCl_3C_{17}H_{11}N_2O_7PZr$ (= YCl_3@ZrO(RP)·py, M_r = 672.71 g mol^{-1}): C 30.35, H 1.65, N 4.16; found: C 29.16, H 2.42, N 4.40; IR: $\tilde{\nu}$ = 3418 (m), 2963 (m), 1613 (w), 1535 (w), 1485 (w), 1413 (w), 1262 (s), 1098 (s), 1022 (s), 801 (s), 676 (w), 485 cm^{-1} (w).

Photoluminescence spectroscopy

Excitation and emission spectra were recorded by using a Horiba Jobin Yvon Fluorolog 3 spectrometer with a 450 W Xe lamp and a FL-1073 photomultiplier tube detector. Emission and excitation wavelengths were monochromatized through Czerny–Turner double gratings (1200 grooves mm^{-1}). An edge filter (400 nm) was used to block the first- and second-harmonic oscillations of the light source. Excitation spectra were recorded from 250 to 580 nm and corrected for the spectral distribution of the lamp by using a photodiode reference detector. Emission spectra were recorded from 380 nm to 800 nm and corrected for the spherical response of the monochromator and the detector using correction spectra provided by the manufacturer. All samples were investigated as dispersions in spectroscopically pure quartz glass cuvettes in front face mode at room temperature.

Sensing of Brønsted acids and bases

ZrO(RP) (3.01 μmol) in pyridine (0.2 mL) was titrated stepwise with defined amounts of NEt_3, water, and HCl (1 μL each: 7.21 μmol NEt_3, 55.5 μmol H_2O, and 1.21 μmol HCl per step). PL excitation and emission spectra were recorded for each step. The compound containing cuvettes were mounted in fixed positions inside the spectrometer to allow for low setup based deviations of PL intensities.

DLS was performed to determine the particle diameter and particle size distribution of the dispersions. Measurements were conducted by using a Malvern Instruments Zetasizer Nano ZS equipped with an He–Ne laser. Detection was carried out by non-invasive backscattering at an angle of 173° with a 256-channel detector.

SEM was performed with a Zeiss Supra 40 VP scanning electron microscope with an acceleration voltage of 5–10 kV and 3 mm working distance. Dispersions were placed on silicon wafers and evaporated.

Acknowledgements

T.W. and K.M.-B. gratefully acknowledge the Volkswagenstiftung for supporting this work within the project 90343 "Multifunctional molecular materials—bridging magnetism and luminescence".

Conflict of interest

The authors declare no conflict of interest.

Keywords: lanthanides · luminescence · nanoparticles · organic–inorganic hybrid composites · sensors

[1] a) M. J. Ruedas-Rama, J. D. Walters, A. Orte, E. A. H. Hall, *Anal. Chim. Acta* **2012**, *751*, 1–23; b) B. Valeur, M. N. Berberan-Santos, *Molecular Fluorescence: Principles and Applications*, Wiley-VCH, Weinheim, **2012**; c) J. F. Callan, A. P. de Silva, D. C. Magri, *Tetrahedron* **2005**, *61*, 8551–8588; d) L. Fabbrizzi, A. Poggi, *Chem. Soc. Rev.* **1995**, *24*, 197–202; e) K. Müller-Buschbaum, F. Beuerle, C. Feldmann, *Microporous Mesoporous Mater.* **2015**, *216*, 171–199.

[2] a) H. He, M. A. Mortellaro, M. J. P. Leiner, R. J. Fraatz, J. K. Tusa, *J. Am. Chem. Soc.* **2003**, *125*, 1468–1469; b) M. N. Stojanovic, P. de Prada, D. W. Landry, *J. Am. Chem. Soc.* **2000**, *122*, 11547–11548; c) D. W. Domaille, E. L. Que, C. J. Chang, *Nat. Chem. Biol.* **2008**, *4*, 168; d) T. Hirano, K. Kikuchi, Y. Urano, T. Higuchi, T. Nagano, *J. Am. Chem. Soc.* **2000**, *122*, 12399–12400.

[3] B. L. Neumeier, M. Khorenko, F. Alves, O. Goldmann, J. Napp, U. Schepers, H. M. Reichardt, C. Feldmann, *ChemNanoMat* **2019**, *5*, 24–45.

[4] a) M. Fehr, W. B. Frommer, S. Lalonde, *Proc. Natl. Acad. Sci. USA* **2002**, *99*, 9846; b) M. Roming, H. Lünsdorf, K. E. J. Dittmar, C. Feldmann, *Angew. Chem. Int. Ed.* **2010**, *49*, 632–637; *Angew. Chem.* **2010**, *122*, 642–647; c) S. M. Buck, H. Xu, M. Brasuel, M. A. Philbert, R. Kopelman, *Talanta* **2004**, *63*, 41–59; d) J. Lu, Z. Rosenzweig, *Fresenius J. Anal. Chem.* **2000**, *366*, 569–575; e) A. Burns, P. Sengupta, T. Zedayko, B. Baird, U. Wiesner, *Small* **2006**, *2*, 723–726.

[5] a) H. Hong, Y. Zhang, J. W. Engle, T. R. Nayak, C. P. Theuer, R. J. Nickles, T. E. Barnhart, W. Cai, *Biomaterials* **2012**, *33*, 4147–4156; b) C. Alric, J. Taleb, G. L. Duc, C. Mandon, C. Billotey, A. L. Meur-Herland, T. Brochard, F. Vocanson, M. Janier, P. Perriat, S. Roux, O. Tillement, *J. Am. Chem. Soc.* **2008**, *130*, 5908–5915; c) Q.-Y. Cai, S. H. Kim, K. S. Choi, S. Y. Kim, S. J. Byun, K. W. Kim, S. H. Park, S. K. Juhng, K.-H. Yoon, *Invest. Radiol.* **2007**, *42*, 797–806.

[6] a) J. A. Barreto, W. O'Malley, M. Kubeil, B. Graham, H. Stephan, L. Spiccia, *Adv. Mater.* **2011**, *23*, H18–H40; b) S. A. Hilderbrand, F. Shao, C. Salthouse, U. Mahmood, R. Weissleder, *Chem. Commun.* **2009**, 4188–4190.

[7] a) J. G. Fujimoto, D. Farkas, *Biomedical Optical Imaging*, Oxford University Press, Oxford, **2009**; b) J. L. West, N. J. Halas, *Annu. Rev. Biomed. Eng.* **2003**, *5*, 285–292; c) M. De, P. S. Ghosh, V. M. Rotello, *Adv. Mater.* **2008**, *20*, 4225–4241.

[8] a) C.-C. Huang, H.-T. Chang, *Anal. Chem.* **2006**, *78*, 8332–8338; b) R. Méallet-Renault, R. Pansu, S. Amigoni-Gerbier, C. Larpent, *Chem. Commun.* **2004**, 2344–2345.

[9] a) R. M. Adhikari, B. K. Shah, S. S. Palayangoda, D. C. Neckers, *Langmuir* **2009**, *25*, 2402–2406; b) A. D. McFarland, R. P. Van Duyne, *Nano Lett.* **2003**, *3*, 1057–1062.

[10] a) Y. Liu, Y. Tang, N. N. Barashkov, I. S. Irgibaeva, J. W. Y. Lam, R. Hu, D. Birimzhanova, Y. Yu, B. Z. Tang, *J. Am. Chem. Soc.* **2010**, *132*, 13951–13953; b) D. E. Achatz, R. J. Meier, L. H. Fischer, O. S. Wolfbeis, *Angew. Chem. Int. Ed.* **2011**, *50*, 260–263; *Angew. Chem.* **2011**, *123*, 274–277.

[11] a) X.-D. Wang, O. S. Wolfbeis, R. J. Meier, *Chem. Soc. Rev.* **2013**, *42*, 7834–7869; b) F. Vetrone, R. Naccache, A. Zamarrón, A. J. de la Fuente, F. Sanz-Rodríguez, L. M. Maestro, E. M. Rodriguez, D. Jaque, J. G. Solé, J. A. Capobianco, *ACS Nano* **2010**, *4*, 3254–3258.

[12] a) Y.-S. Liu, Y. Sun, P. T. Vernier, C.-H. Liang, S. Y. C. Chong, M. A. Gundersen, *J. Phys. Chem. C* **2007**, *111*, 2872 – 2878; b) F. Gao, L. Tang, L. Dai, L. Wang, *Spectrochim. Acta Part A* **2007**, *67*, 517 – 521.
[13] S. J. Toal, K. A. Jones, D. Magde, W. C. Trogler, *J. Am. Chem. Soc.* **2005**, *127*, 11661 – 11665.
[14] H. Li, L. Wang, *Analyst* **2013**, *138*, 1589 – 1595.
[15] a) K. P. Carter, A. M. Young, A. E. Palmer, *Chem. Rev.* **2014**, *114*, 4564 – 4601; b) H. Y. Au-Yeung, J. Chan, T. Chantarojsiri, C. J. Chang, *J. Am. Chem. Soc.* **2013**, *135*, 15165 – 15173; c) S. D. Lytton, B. Mester, J. Libman, A. Shanzer, Z. I. Cabantchik, *Anal. Biochem.* **1992**, *205*, 326 – 333; d) X. Mao, H. Su, D. Tian, H. Li, R. Yang, *ACS Appl. Mater. Interfaces* **2013**, *5*, 592 – 597; e) G. K. Walkup, S. C. Burdette, S. J. Lippard, R. Y. Tsien, *J. Am. Chem. Soc.* **2000**, *122*, 5644 – 5645.
[16] a) I. L. Medintz, H. T. Uyeda, E. R. Goldman, H. Mattoussi, *Nat. Mater.* **2005**, *4*, 435; b) F. Ye, C. Wu, Y. Jin, Y.-H. Chan, X. Zhang, D. T. Chiu, *J. Am. Chem. Soc.* **2011**, *133*, 8146 – 8149.
[17] a) R. Chen, V. D. Ta, F. Xiao, Q. Zhang, H. Sun, *Small* **2013**, *9*, 1052 – 1057; b) L. H. Fischer, G. S. Harms, O. S. Wolfbeis, *Angew. Chem. Int. Ed.* **2011**, *50*, 4546 – 4551; *Angew. Chem.* **2011**, *123*, 4640 – 4645.
[18] a) C. D. S. Brites, P. P. Lima, N. J. O. Silva, A. Millán, V. S. Amaral, F. Palacio, L. D. Carlos, *Adv. Mater.* **2010**, *22*, 4499 – 4504; b) H. Peng, M. I. J. Stich, J. Yu, L.-N. Sun, L. H. Fischer, O. S. Wolfbeis, *Adv. Mater.* **2010**, *22*, 716 – 719.
[19] T. Wehner, J. Heck, C. Feldmann, K. Müller-Buschbaum, *J. Mater. Chem. C* **2016**, *4*, 7735 – 7743.
[20] a) T. Thongtem, S. Kungwankunakorn, B. Kuntalue, A. Phuruangrat, S. Thongtem, *J. Alloys Compd.* **2010**, *506*, 475 – 481; b) T. Grzyb, S. Lis, *J. Rare Earths* **2009**, *27*, 588 – 592.
[21] A. S. Susha, A. M. Javier, W. J. Parak, A. L. Rogach, *Colloids Surf. A* **2006**, *281*, 40 – 43.
[22] W. Shi, X. Li, H. Ma, *Angew. Chem. Int. Ed.* **2012**, *51*, 6432 – 6435; *Angew. Chem.* **2012**, *124*, 6538 – 6541.
[23] H. Sun, A. M. Scharff-Poulsen, H. Gu, K. Almdal, *Chem. Mater.* **2006**, *18*, 3381 – 3384.
[24] a) Y. Wu, G.-P. Yang, Y. Zhao, W.-P. Wu, B. Liu, Y.-Y. Wang, *Dalton Trans.* **2015**, *44*, 3271 – 3277; b) Q. Tang, S. Liu, Y. Liu, J. Miao, S. Li, L. Zhang, Z. Shi, Z. Zheng, *Inorg. Chem.* **2013**, *52*, 2799 – 2801.
[25] a) Z. Guo, H. Xu, S. Su, J. Cai, S. Dang, S. Xiang, G. Qian, H. Zhang, M. O'Keeffe, B. Chen, *Chem. Commun.* **2011**, *47*, 5551 – 5553; b) J.-H. Wang, M. Li, D. Li, *Chem. Sci.* **2013**, *4*, 1793 – 1801; c) Y.-N. Gong, T.-B. Lu, *Chem. Commun.* **2013**, *49*, 7711 – 7713.
[26] J. Aguilera-Sigalat, D. Bradshaw, *Chem. Commun.* **2014**, *50*, 4711 – 4713.
[27] Y. Cui, H. Xu, Y. Yue, Z. Guo, J. Yu, Z. Chen, J. Gao, Y. Yang, G. Qian, B. Chen, *J. Am. Chem. Soc.* **2012**, *134*, 3979 – 3982.
[28] a) Z. Hu, B. J. Deibert, J. Li, *Chem. Soc. Rev.* **2014**, *43*, 5815 – 5840; b) J. Heine, K. Müller-Buschbaum, *Chem. Soc. Rev.* **2013**, *42*, 9232 – 9242.
[29] a) D. Liu, K. Lu, C. Poon, W. Lin, *Inorg. Chem.* **2014**, *53*, 1916 – 1924; b) M. H. Keefe, K. D. Benkstein, J. T. Hupp, *Coord. Chem. Rev.* **2000**, *205*, 201 – 228; c) A. P. de Silva, D. B. Fox, T. S. Moody, S. M. Weir, *Pure Appl. Chem.* **2001**, *73*, 503 – 511.
[30] a) Y. Li, S. Zhang, D. Song, *Angew. Chem. Int. Ed.* **2013**, *52*, 710 – 713; *Angew. Chem.* **2013**, *125*, 738 – 741; b) J. Wang, L. Long, D. Xie, Y. Zhan, *J. Lumin.* **2013**, *139*, 40 – 46; c) X. Cao, W. Lin, L. He, *Org. Lett.* **2011**, *13*, 4716 – 4719.
[31] a) L. Li, G. Wu, T. Hong, Z. Yin, D. Sun, E. S. Abdel-Halim, J.-J. Zhu, *ACS Appl. Mater. Interfaces* **2014**, *6*, 2858 – 2864; b) T. N. J. I. Edison, R. Atchudan, J.-J. Shim, S. Kalimuthu, B.-C. Ahn, Y. R. Lee, *J. Photochem. Photobiol. B* **2016**, *158*, 235 – 242; c) T. Wehner, K. Mandel, M. Schneider, G. Sextl, K. Müller-Buschbaum, *ACS Appl. Mater. Interfaces* **2016**, *8*, 5445 – 5452.
[32] A. P. de Silva, T. S. Moody, G. D. Wright, *Analyst* **2009**, *134*, 2385 – 2393.
[33] a) T. Wehner, M. T. Seuffert, J. R. Sorg, M. Schneider, K. Mandel, G. Sextl, K. Müller-Buschbaum, *J. Mater. Chem. C* **2017**, *5*, 10133 – 10142; b) Y. Takashima, V. M. Martínez, S. Furukawa, M. Kondo, S. Shimomura, H. Uehara, M. Nakahama, K. Sugimoto, S. Kitagawa, *Nat. Commun.* **2011**, *2*, 168; c) Z. Xu, Y. Xiao, X. Qian, J. Cui, D. Cui, *Org. Lett.* **2005**, *7*, 889 – 892.
[34] J. G. Heck, J. Napp, S. Simonato, J. Möllmer, M. Lange, H. M. Reichardt, R. Staudt, F. Alves, C. Feldmann, *J. Am. Chem. Soc.* **2015**, *137*, 7329 – 7336.
[35] P. D. McQueen, S. Sagoo, H. Yao, R. A. Jockusch, *Angew. Chem. Int. Ed.* **2010**, *49*, 9193 – 9196; *Angew. Chem.* **2010**, *122*, 9379 – 9382.
[36] Z. Liu, W. He, Z. Guo, *Chem. Soc. Rev.* **2013**, *42*, 1568 – 1600.
[37] S. Cotton, *Lanthanides and Actinides*, Macmillan Education, London, **1991**.
[38] a) L. S. Forster, D. Dudley, *J. Phys. Chem.* **1962**, *66*, 838 – 840; b) S. Guo, Y. Ma, S. Liu, Q. Yu, A. Xu, J. Han, L. Wei, Q. Zhao, W. Huang, *J. Mater. Chem. C* **2016**, *4*, 6110 – 6116; c) M. P. Lettinga, H. Zuilhof, M. A. M. J. van Zandvoort, *Phys. Chem. Chem. Phys.* **2000**, *2*, 3697 – 3707.
[39] a) V. S. Pavlovich, *ChemPhysChem* **2012**, *13*, 4081 – 4093; b) F. Naderi, A. Farajtabar, F. Gharib, *J. Mol. Liq.* **2014**, *190*, 126 – 132; c) B. Acemioğlu, M. Arık, H. Efeoğlu, Y. Onganer, *J. Mol. Struct.* **2001**, *548*, 165 – 171.
[40] M. F. Choi, P. Hawkins, *Spectrosc. Lett.* **1994**, *27*, 1049 – 1063.
[41] T. Tang, Y.-Q. Chen, B.-S. Fu, Z.-Y. He, H. Xiao, F. Wu, J.-Q. Wang, S.-R. Wang, X. Zhou, *Chin. Chem. Lett.* **2016**, *27*, 540 – 544.
[42] K. N. Bobba, Y. Zhou, L. E. Guo, T. N. Zang, J. F. Zhang, S. Bhuniya, *RSC Adv.* **2015**, *5*, 84543 – 84546.
[43] K. Cui, Z. Chen, Z. Wang, G. Zhang, D. Zhang, *Analyst* **2011**, *136*, 191 – 195.
[44] M. Roming, C. Feldmann, *Solid State Sci.* **2011**, *13*, 508 – 512.
[45] M. D. Taylor, C. P. Carter, *J. Inorg. Nucl. Chem.* **1962**, *24*, 387 – 391.

Manuscript received: August 16, 2019
Revised manuscript received: October 14, 2019
Accepted manuscript online: October 18, 2019
Version of record online: December 9, 2019

